

Addressing γ -ray emissions from dark matter annihilations in 45 milky way satellite galaxies and in extragalactic sources with particle dark matter models

Ashadul Halder* and Shibaji Banerjee†

Department of Physics, St. Xavier's College, 30, Mother Teresa Sarani, Kolkata-700016, India.

Madhurima Pandey‡ and Debasish Majumdar§

*Astroparticle Physics and Cosmology Division, Saha Institute of Nuclear Physics,
HBNI, 1/AF Bidhannagar, Kolkata 700064, India*

The mass to luminosity ratio of the dwarf satellite galaxies in the Milky Way suggests that these dwarf galaxies may contain substantial dark matter. The dark matter at the dense region such as within or at the vicinity of the centres of these dwarf galaxies may undergo the process of self annihilation and produce γ -rays as the end product. The satellite borne γ -ray telescope such as *Fermi*-LAT reported the detection of γ -rays from around 45 Dwarf Spheroidals (dSphs) of Milky Way. In this work, we consider particle dark matter models described in the literature and after studying their phenomenologies, we calculate the γ -ray fluxes from the self annihilation of the dark matter within the framework of these models in case of each of these 45 dSphs. we then compare the computed results with the observational upper bounds for γ -ray flux reported by *Fermi*-LAT and Dark Energy Survey (DES) for each of the 45 dSphs. The fluxes are calculated by adopting different dark matter density profiles. We then extend similar analysis for the observational upper bounds given by *Fermi*-LAT for the continuum γ -ray fluxes originating from extragalactic sources.

Keywords: galaxies: dwarf – galaxies: structure – dark matter – gamma-rays: galaxies – gamma-rays: general – gamma-rays:ISM

arXiv:1910.02322v3 [astro-ph.CO] 12 Jan 2021

* ashadul.halder@gmail.com

† shiva@sxccal.edu

‡ madhurima.pandey@saha.ac.in

§ debasish.majumdar@saha.ac.in

I. INTRODUCTION

Although the existence of dark matter (DM) in the Universe is now well established, any direct signature of the dark matter is still eluding the worldwide endeavours at different direct dark matter search experiments. The indirect search for dark matter involves detection of the known Standard Model (SM) particles that can be produced by possible dark matter annihilation (or decay) in cosmos. Although the cosmic relics, the dark matter can undergo self annihilation if it is accumulated in considerable magnitude by being captured, under the influence of gravity, inside massive astrophysical bodies. In literature there are indications that the emissions of excess γ -rays from the Galactic Centre (GC) region (detected by *Fermi*-LAT satellite borne experiment) could have been originated from the annihilation of dark matter at GC region. The dwarf spheroidals are the satellite galaxies to the Milky Way and they fail to grow as matured galaxies. These dwarf spheroidal galaxies (dSphs) are generally of low luminosities and contain population of older stars with little dust. The dwarf spheroidals could be very rich in dark matter. These galaxies would have been tidally disrupted but the presence of dark matter provides the necessary gravitational pull. The existence of dark matter in dwarf spheroidals can also be realised by studying their mass to luminosity ratios. From several observations the estimated mass to luminosity ratios (M/L) are found to be much more than the same for the sun ($|\frac{M}{L}|$). The dark matter at dSphs can undergo self annihilation and produce γ -rays.

The *Fermi*-LAT satellite borne observations and Dark Energy Survey (DES) have reported the upper bounds of the γ -ray spectra for several dwarf galaxies [3, 6]. Here in this work, we consider two particle dark matter models (one is the simple extension of Standard Model and the other is inspired by a Beyond Standard Model (BSM) theory of particle physics) and for the dark matter candidates in each of these two models, we compute the expected γ -ray flux from all the 45 dSphs mentioned above by considering the dark matter annihilations at those dSphs. These computed results are then compared with the observational upper bounds for γ -ray flux for each of the 45 dSphs. The *Fermi*-LAT experiment also provides [1, 4] the observational results for extragalactic γ -ray flux. If the γ -rays (or a component of that) also originate from dark matter annihilation, then this too could be indirect signal of dark matter. The dark matter annihilation to γ -rays in extragalactic source is considered to add to the extragalactic γ -ray flux. To this end, we compute the extragalactic γ -ray flux from other possible sources such as GRB, BL Lacs etc. and add to them the possible contribution to extragalactic γ -rays from dark matter annihilations (within the framework of the dark matter models considered in this work). We then compare the sum total flux with *Fermi*-LAT results.

The first (Model I) of the two models are chosen based on the following considerations. It has been shown earlier, in the context of explaining the observed excess in Galactic Centre γ -ray signal within the energy range of around 2-8 GeV, that this excess can be well explained from the annihilation of WIMP (Weakly Interacting Massive Particle) dark matter of mass in the range of tens of GeV [10, 12, 28, 29] which annihilates principally to $b\bar{b}$ as primary products with the dark matter annihilation cross-section $\langle\sigma v\rangle$ (v represents the velocity of dark matter) in the ball park of 10^{-26} cm³ s⁻¹. The first model for particle dark matter considered in this work is inspired by Dutta Banik *et al.* [24]. It has been demonstrated [24] that the WIMP dark matter component of this first model (describe later) satisfies these criteria along with the criteria for dark matter relic density given by Planck satellite borne experiment [49] based on the observation and analysis of the anisotropies of Cosmic Microwave Background Radiation (CMBR). This has also been shown in Dutta Banik *et al.* [24] that the WIMP component (of mass ~ 50 GeV) in their two component dark matter model (adopted here as Model I) can well explain the observed Galactic Centre γ -ray fluxes observed by *Fermi*-LAT from this region. The dark matter candidate in the second model (Model II) adopted here is inspired by an established beyond Standard Model (BSM) theory namely theory of universal extra dimension [18]. This has been shown by [37, 53], that the dark matter mass in this model should be around 900 GeV in order that calculated relic density for such a dark matter in this model satisfies Planck relic density results. Being in a mass regime higher than that for the dark matter candidate in Model I, the γ ray spectrum originated from this dark matter annihilation will have a wider energy range and thus raises the possibility of exploring the whole energy range given by the *Fermi*-LAT observed results for the upper bound of the γ -ray flux from all the 45 dwarf galaxies considered in this work. The same particle dark matter formalism is then adopted for the extragalactic γ -ray case.

The first (Model I) of the two particle dark matter models mentioned above is a two component dark matter model (obtained by minimal extension of Standard Model) where one component is a Feebly Interacting Massive particle or FIMP (we have denoted FIMP as FImP for being less massive) and the other component is a Weakly Interacting Massive Particle or WIMP. The model is proposed and its phenomenology is elaborately worked out in an earlier work involving two of the present authors (Ref. [24]). While the FImP component of this two component dark matter model could explain the phenomena such as dark matter self interactions, the WIMP component was useful in explaining the excess γ -rays from GC region when they annihilate mainly into $b\bar{b}$ to finally produce γ -rays. The model is constructed by minimal extension of Standard Model with a Dirac fermion χ , a real scalar S and a pseudoscalar ϕ . While the fermion χ and the scalar S are singlets under SM gauge group, the fermion has an additional $U(1)_{\text{DM}}$ charge. This prevents the fermion χ to interact with SM fermions ensuring stability. A Z_2 symmetry is imposed on the scalar S . The Lagrangian is CP invariant but the CP invariance is broken when the pseudoscalar ϕ acquires a vacuum

expectation value (vev). On the other hand, the scalar develops a vev when the Z_2 symmetry is spontaneously broken. Thus after spontaneous breaking of the symmetries $(SU(2)_L \times U(1)_Y, Z_2, CP)$, the scalars in the theory namely the Higgs H , S and ϕ acquire vev and their real components mix together. Three mass eigen states h_1 , h_2 and h_3 are obtained (small mixing angles, $\theta_{12} \sim 10^{-2}$, $\theta_{13} \sim 10^{-13}$ and $\theta_{23} \sim 10^{-15}$) after diagonalisation of mass matrix while eigen state h_1 is identified with the physical Higgs with mass 125.5 GeV, h_2 is identified with the pseudo scalar considered in the model. Since h_1 is identified with SM Higgs, one requires to consider the collider bounds for the limit on R_1 (SM Higgs signal strength) which is expressed as the ratio of total decay width of the SM Higgs and the calculated total decay width of h_1 . One also requires to consider invisible decay branching ratio (Br_{inv}^1) of SM like Higgs h_1 and this parameter is fixed using collider constrains. The lightest mass eigenstate after diagonalisation (with small mixing with other scalars) is taken to be the FIMP candidate. But in this work, in order to calculate the γ -rays from the annihilation of dark matter in each of the chosen 45 dwarf galaxies (as also the extragalactic γ -ray case), the WIMP component which is the Dirac singlet fermion (in this WIMP-FIMP model) is useful. The WIMP candidate in this model interacts with SM sector through Higgs portal. In Ref. Dutta Banik *et al.* [24], this has been shown that the excess γ -rays from the Galactic Centre within the energy range 2 GeV - 8 GeV as reported by *Fermi*-LAT can be well explained by the WIMP component (fermion χ) of this WIMP-FIMP model if the WIMPs (χ) self annihilate to $b\bar{b}$ which in turn produces secondary γ -rays. The cross-section for the channel $\chi\chi \rightarrow b\bar{b}$ is calculated and computed in Ref. Dutta Banik *et al.* [24] for certain model benchmark points. The computations of annihilation cross-section of the process $\chi\chi \rightarrow b\bar{b}$ require the coupling and other factors (the expression for this cross-section is given in Appendix of Dutta Banik *et al.* [24]) to be determined by constraining the model interaction lagrangian with theoretical bounds as well as experimental bounds and collider bounds. The process $\chi\chi \rightarrow b\bar{b}$ is mediated by the scalar h_1 and h_2 and one needs the coupling 'g' of the pseudo scalar (h_2) with the dark matter fermion χ as also the other couplings of χ with h_1 . The coupling g is a parameter in this model (the expression of the couplings of the fermions with Higgs are known). Again since Model I is two component dark matter model (the WIMP component of which is considered here (similar to what is considered in Dutta Banik *et al.* [24])), the fraction of WIMP component χ that contributes to generate required Galactic Centre γ -ray excess in Dutta Banik *et al.* [24] is denoted by f_χ . The annihilation cross-section $\langle\sigma v\rangle_{\chi\chi \rightarrow b\bar{b}}$ will also be weighted by this fraction f_χ . Thus f_χ is also a parameter of the model. The allowed ranges of all these parameters are obtained by constraining the model interaction lagrangian with theoretical (unitarity, perturbativity etc.) as well as experimental constraints (e.g. PLANCK relic density results) and collider constraints. In Ref. Dutta Banik *et al.* [24] the several benchmark values of model parameters are given for computing the Galactic Centre γ -ray excess and comparing with the *Fermi*-LAT results for the same. In the present work, we adopt one of such benchmark point and compute the γ -ray fluxes for all the 45 dSphs by similar consideration of annihilation of the WIMP component χ (of the two component model discussed above) to $b\bar{b}$ and compare them with upper bounds of all those 45 dSphs given by *Fermi*-LAT experiment [3, 6]. This benchmark point (set of values of the parameters) are shown in Table I. The astrophysical \mathcal{J} -factor values required to compute the fluxes are obtained from different observational groups for the dwarf galaxies.

The other particle dark matter candidate considered in this work is from a BSM theory and this candidate is Kaluza-Klein (KK) dark matter (Model II) inspired by the theories of extra dimensions [18, 30, 37, 53]. If only one spatial extra dimension is considered and this extra dimension is compactified over a circle of compactification radius R , say, then the effective four dimensional theory as obtained by integrating the extra spatial dimension over the periodic coordinate ($y \rightarrow y + 2\pi R$), compactification over a circle, gives rise to a tower of Kaluza-Klein modes with mass of each mode given by $m_k = k/R$, where k is called the Kaluza-Klein number or KK number. As KK number is associated with the quantized momentum in compactified dimension ($E^2 = \mathbf{p}^2 + m_k^2$), the KK number is conserved and hence the Lightest Kaluza-Klein particle or LKP is stable and can be a candidate for dark matter.

In this work, we consider a KK dark matter candidate in an extra dimensional model namely Universal Extra Dimensional model (UED) [8, 18, 34, 53]. In this model, each of the SM field can propagate in the extra dimension and every SM particle has a KK tower. But since the SM fermions are chiral, in order to obtain chiral KK counterpart of the SM fermions in UED model, the compactification of the extra dimension is to be made over a S^1/Z_2 orbifold (instead of compactifying just over a circle S^1 with compactification radius R) where a reflection symmetry Z_2 is imposed under which the extra coordinate $y \rightarrow -y$ and the fields are even or odd. Thus the chirality of a fermion can be identified in the extra dimension. The orbifold has now two boundary points at 0 and πR . But this breaks translational symmetry in the y direction and the KK momentum is no more conserved. Therefore the KK number (k) is also not conserved and the LKP is no more stable. But, for the transformation $y \rightarrow y + \pi R$, the KK modes remain invariant for even KK number but odd KK modes change sign. Thus we have a quantity called $(-1)^{KK}$ - the KK parity - which is a good symmetry for this transformation and hence conserved. The conservation of KK parity ensures LKP in UED model is stable. In the present work, the LKP dark matter candidate in UED model is the first KK partner B^1 of the hypercharge gauge boson.

We have taken a range of masses for the chosen KK dark matter candidate B^1 and demonstrate how well the γ -rays produced from the annihilation of such a dark matter candidate agrees with the observational results for all the dwarf

TABLE I. The model parameter considered for the calculation on γ -ray fluxes in Model I. v_1 is the vev of SM Higgs.

M_χ	v_1	g	R_1	Br_{inv}^1	f_χ	$f_\chi^2 \langle \sigma v \rangle_{b\bar{b}}$
GeV	GeV					$10^{-26} \text{cm}^3 \text{s}^{-1}$
50	246	0.11	0.99	0.021	0.89	1.62

galaxies considered. The range of masses for these KK particles are so chosen that the PLANCK limits for the dark matter relic densities are satisfied. For continuum γ signal from $B^1 B^1$ annihilation one needs to consider the channel $B^1 B^1 \rightarrow qq$ (q denotes the quarks). The annihilation cross-sections ($\langle \sigma_{qq} v \rangle$) for this channel are calculated following [18]. It is to be noted that the interaction coupling for the process $B^1 B^1 \rightarrow qq$ is computable for a given mass of the dark matter candidate B^1 [18]. The only parameter here is the mass of q^1 which is the first KK partner of quark q in the UED model. The parameter is rewritten as $r = \frac{m_{q^1} - m_{B^1}}{m_{B^1}}$, where, m_{q^1} , m_{B^1} are the masses of q^1 and B^1 respectively. In this work, we have varied parameter r in such a way that m_{B^1} is in the allowed mass range (discussed earlier) and $m_{q^1} > m_{B^1}$ is maintained. We do not find any significant changes in the result.

We then extend our analyses for extragalactic γ -rays also. The observed extragalactic γ -ray signal may contain the component of γ -ray from dark matter annihilations at extragalactic sources ([11, 27, 44, 56, 58, 59]). The extragalactic γ -rays can have many components other than those possibly from dark matter annihilations. There are attempts to extract dark matter annihilation signals from the extragalactic γ -ray background or EGB [2, 5, 15, 19, 21, 22, 52, 57]. The possible contribution to the EGB may come from BL Lac objects, millisecond pulsars, radio galaxies etc. More detailed knowledge and their possible contribution to the EGB not only helps to look for any such dark matter annihilation signals beyond the EGB but also is useful to put stringent bound on dark matter annihilation cross-sections. With both the particle dark matter models considered here, we have made an attempt in this work to estimate whether any significant signal from the dark matter annihilation can be obtained from extragalactic sources. For the extragalactic also, the same benchmark points given in Table I and Table III are used.

In an earlier work ([39]), similar analyses have been performed. But in that analyses only 18 dSphs were considered with inert doublet dark matter but in the preset analyses we take into account as many as 45 dSphs. Also, in this work, two dark matter models are considered under which one dark matter candidate is the Higgs portal component of a two component DM ([24]) while the other is a particle dark matter inspired by theories of extra dimensions ([18, 30, 37, 53]).

The paper is organised as follows. In Sect. II we give the formalism to calculate γ -ray flux. Sect. III deals with the observational data, the calculations and results for the dwarf galaxies and the comparison of the computed results with observational bounds. The calculational procedures for the estimation of extra galactic γ -ray background and the contribution from possible dark matter annihilation are given in Sect. IV. Finally in Sect. V we conclude with a summary and some remarks.

II. FORMALISM FOR γ -RAY FLUX CALCULATIONS IN CASE OF DWARF GALAXIES FROM DARK MATTER ANNIHILATION

The observed flux from cosmic dark matter source depends significantly on the dark matter annihilation cross-section $\langle \sigma v \rangle$ [3] as well as the total DM contained within the solid angle subtended by the source at the observer (the astrophysical \mathcal{J} -factor). Analytically the \mathcal{J} -factor can be calculated as

$$\mathcal{J} = \int_{l.o.s} \rho(r)^2 ds = r_\odot \rho_\odot^2 J. \quad (1)$$

In the above, ρ_\odot ($0.3 \text{ GeV}/\text{cm}^3$) is the dark matter density at the distance r_\odot (8.33 kpc) from the Galactic Centre (at the solar system). In the above equation, J represents the dimensionless form of \mathcal{J} -factor given by,

$$J = \int_{l.o.s} \frac{1}{r_\odot} \left(\frac{\rho(r)}{\rho_\odot} \right)^2 ds, \quad (2)$$

where $\rho(r)$ is the DM density at radial distance r from the Galactic Centre and $\rho(r)$ in a dark matter halo can be parametrised as $\rho(r) = \rho_s g(r/r_s)$, where ρ_s is a scale density and $g(r/r_s)$ gives the nature of density function with r and r_s is a characteristic scale distance. In this case $r_s = 20 \text{ kpc}$ for dwarf galaxy calculations. The radial distance r

TABLE II. Dark matter halo profiles

NFW [41, 42]	$\rho_{\text{NFW}} = \rho_s \frac{r_s}{r} \left(1 + \frac{r}{r_s}\right)^{-2}$
Einasto [25]	$\rho_{\text{Ein}} = \rho_s \exp \left[-\frac{2}{\alpha} \left\{ \left(\frac{r}{r_s}\right)^\alpha - 1 \right\} \right]$
Burkert [17, 51]	$\rho_{\text{Bur}} = \frac{\rho_s}{(1+r/r_s)(1+(r/r_s)^2)}$

can be expressed in terms of the line of sight s as,

$$r = \begin{cases} \sqrt{s^2 + r_\odot^2 - 2sr_\odot \cos l \cos b} & l, b \text{ coordinate,} \\ \sqrt{s^2 + r_\odot^2 - 2sr_\odot \cos \theta} & r, \theta \text{ coordinate.} \end{cases} \quad (3)$$

We adopt three density profiles for computation of $\rho(r)$ and those three profiles are given in Table II.

The differential γ -ray flux due to dark matter annihilation of mass M_χ is given by [20],

$$\frac{d\phi}{d\Omega dE_\gamma} = \frac{1}{8\pi\alpha} \sum_f \frac{\langle\sigma v\rangle_f}{M_\chi^2} \frac{dN_\gamma^f}{dE_\gamma} \mathcal{J}, \quad (4)$$

where $\alpha = 1$ and f indicates the final state particle.

As mentioned earlier, we have considered two particle dark matter models in this work. One is a two component WIMP-FIMP model where the WIMP component χ of mass around 50 GeV (Table I) contributes to γ -rays (Model I) by their self annihilation (via a Higgs portal) leading primarily to $b\bar{b}$. The expression of the cross-section for the process $\chi\chi \rightarrow b\bar{b}$ is given in the Appendix of [24]. The annihilation cross-section is computed to be $\langle\sigma v\rangle = 1.62 \times 10^{-26} \text{cm}^3 \text{sec}^{-1}$. The computations of annihilation cross-section require numerical values of the various couplings involved in different interactions. These couplings are the particle dark matter model parameters and are discussed in Dutta Banik *et al.* [24]. In Table I we furnish a set of benchmark values taken from the allowed region of these parameters discussed in Dutta Banik *et al.* [24]. The set of values of the couplings is used in present work. It is to be noted that, these coupling parameters are in agreement with the bounds and the constraints coming from the theoretical considerations such as vacuum stability conditions, perturbativity and unitarity conditions etc. and they also satisfy the various bounds given by the experimental observations, e.g., the collider physics bounds (LHC bounds), the PLANCK observational results for the dark matter relic density and the upper limit on the dark matter - nucleon scattering cross-section obtained from different dark matter direct detection experiments. All the above mentioned constraints and bounds imposed on the model parameters (such as various interaction couplings etc.) which are necessary in order to compute the annihilation cross-section for the channel $\chi\chi \rightarrow b\bar{b}$, have been elaborately discussed in [24]. The parameters in Table I are within the allowed range of model parameter space and they also respect all the necessary constraints and bounds. Same set of coupling parameter value and the same formalism are adopted for extragalactic case also.

The other is a KK dark matter (B^1) in an extra dimensional model (Model II) having a mass of about 900 GeV (Table III) which self annihilates to the primary product qq and yields γ -rays as the end product. For the case of B^1 dark matter, the annihilation cross-section $B^1 B^1 \rightarrow qq$ is computed from the expression [18]

$$\langle\sigma_{qqv}\rangle = \frac{q^4}{9\pi \cos^4 \theta_W} \left[\frac{Y_{q_L}^4}{m_{B^1}^2 + m_{q_L}^2} + L \rightarrow R \right] \quad (5)$$

where q_L^1 is the first KK partner of the quark q_L , $Y_{q_L}^1$ and $m_{q_L}^1$ are respectively the corresponding hypercharge and mass while θ_W is the Weinberg angle. The mass $m_{q_L}^1$ are fixed by defining a parameter $r = (m_{q^1} - m_{B^1})/m_{B^1}$ ([18]) and then adopting a suitable value for r . It is also to be noted that the LKP dark matter candidate B^1 in this case is the first KK partner of the hypercharge gauge boson. It is seen that the mass of this dark matter candidate should be ~ 900 GeV for its relic density to satisfy the PLANCK result [49]. In the limit in which electroweak symmetry breaking (EWSB) is neglected, there will be no channels with vector gauge bosons as primary products and only 2% of the annihilation goes into Higgs [53]. Moreover [18] shows that the channel $B^1 B^1 \rightarrow e^+ e^-$ yields narrow peaks for positrons and for computation of continuum photon signal the relevant annihilation cross-section is $\langle\sigma_{qqv}\rangle$. The choice of dark matter masses in both the models are shown in Table III. Same formalism of dark matter annihilation with same dark matter mass is adopted for the extragalactic γ -ray flux calculations.

The γ fluxes are calculated (for the chosen dark matter candidates) by computing the \mathcal{J} factor with each of the three density profiles of Table II. The fluxes are also computed with the \mathcal{J} factors estimated and published by other groups [13, 46]. These density profiles are plotted in Fig. 1.

TABLE III. The masses of the dark matter in both the models adopted in the work.

Model	M_χ in GeV
Model I ([24])	50
Model II ([18, 53])	900

III. THE γ -RAY FLUX CALCULATIONS FOR THE DWARF GALAXIES AND THEIR COMPARISON WITH THE OBSERVATIONS

DM rich dwarf spheroidal galaxies (dSphs) have turned out to be important cosmological sites to probe and understand the nature of dark matter and its astrophysical implications. The satellite observations by *Fermi*-LAT [9] as well as later Dark Energy Survey (DES) and *Fermi*-LAT collaboration reveal a sum of 45 dwarf spheroidal galaxies in the energy range $0.5 \sim 500$ GeV [3]. The details of these dSphs are furnished in Table IV. In Table IV the \mathcal{J} factors and their uncertainties are also given for those 45 dSphs. These *Fermi*-LAT observations upper bounds are obtained from [3, 6]. The upper bounds of γ -ray fluxes from those dSphs are given in Fig. 2.

In the present work we have estimated γ -flux for all of those 45 dSphs tabulated in Table IV assuming that the dark matter in those dSphs annihilate to produce γ . The computations for γ flux for each of the two DM candidates have been performed following Eqs. (1) - (5). The DM candidates and models as also the chosen DM masses are already discussed and in Table III the benchmark mass points are given. Note that the cross-section given in Eq. 5 is for KK dark matter only (Model II).

Figs. 2 and 3 show upper bound of γ -ray flux given by the *Fermi*-LAT observation as well as the computed γ -ray flux for the two particle dark matter candidates. In Figs. 2 and 3 the upper bound of the γ -ray flux for all the 45 galaxies (as given by *Fermi*-LAT collaboration) are shown with green arrows pointing downwards. Integrated \mathcal{J} -factor over a solid angle of $\Delta\Omega = 2.4 \times 10^{-4}$ sr (field of view of *Fermi*-LAT $\sim 0.5^\circ$) are measured from stellar kinematics data. The numerical values of \mathcal{J} -factor for all dSphs (obtained from observational data) are tabulated in Table IV.

The computations of flux for the DM candidates in both the models are made as follows. Integrated \mathcal{J} -factor over a solid angle of $\Delta\Omega = 2.4 \times 10^{-4}$ sr (field of view of *Fermi*-LAT $\sim 0.5^\circ$) are measured from stellar kinematics data. The numerical values of \mathcal{J} -factor for all dSphs (obtained from observational data) as well as the flux estimations for the case of both the models I and II using the \mathcal{J} -factors are tabulated in Table IV. The flux estimations for the case of both the Models I and II are first made using the \mathcal{J} factors given in Table IV. The spread of each of these calculated fluxes due to the uncertainties of the \mathcal{J} factors (given in Table IV) are also calculated in case of each of the two dark matter models considered. The fluxes and their spreads thus estimated with both the DM candidates for all the 45 dSphs are shown in Figs. 2 and 3. The γ flux for DM in Model I (WIMP component χ with mass ~ 50 GeV of two component WIMP-FImP model) are shown by a black line (for the central values of \mathcal{J} in Table IV) and the estimated spread of these computed fluxes due to uncertainties in corresponding \mathcal{J} values are shown by yellow bands in each of the 45 plots (for 45 dwarf galaxies) spreaded over Figs. 2 and 3. Similar estimations of the γ flux and their uncertainties for the DM candidate B^1 (KK dark matter from extra dimensional model with mass ~ 900 GeV; Model II) are shown with blue central lines with uncertainty spreads shown in pink in each of the 45 plots (of Figs. 2 and 3).

The fluxes are also estimated for both the dark matter candidates (Model I and Model II) following Eqs. 1-4 by explicitly computing the \mathcal{J} with each of the three dark matter density profiles given in Table II. These are NFW, Einasto and Burkert DM density profiles. They are shown in Figs. 2 and 3 in red, black and blue dashed lines respectively for the WIMP dark matter in Model I and in red, black and blue dotted lines for the KK dark matter of Model II. It can be seen that for most of the cases, the results using NFW profiles almost coincide with those using Einasto profile while distinction can be made for the flux results with Burkert profile. This may be understood from the natures of the profiles (Fig. 1). While both NFW and Einasto profiles are cuspy in nature, the Burkert profile is flat and isothermal in nature. Also Burkert profile has been used earlier to analyse the dwarf galaxy rotation curves ([17, 35]).

It appears from Figs. 2 and 3 that for Model I (the WIMP component of a WIMP-FImP model) with all the three density profiles, the fluxes are below the observational upper limits of all the 45 dSphs. Similar results for the KK dark matter in Model II (the Kaluza-Klein model) are shown in Figs. 2 and 3 with colour codes mentioned above. It can be seen that KK dark matter also respects the observational upper bounds of all the dSphs γ -fluxes considered here. Moreover, it can also be seen from Figs. 2 and 3 that wider range (in comparison to what obtained in case of Model I) of γ -ray flux can be achieved when KK dark matter (Model II) is considered.

TABLE IV. Latitude, longitude, distance and \mathcal{J} -factor for individual dSphs [13, 46].

dSphs name	Longitude l (deg)	Latitude b (deg)	Distance (kpc)	$\log_{10} \mathcal{J}$ ($\log_{10} [\text{GeV}^2 \text{cm}^{-5} \text{sr}]$)
Bootes I	358.1	69.6	66	18.17 ± 0.30
Bootes II	353.7	68.9	42	18.90 ± 0.60
Bootes III	35.4	75.4	47	18.80 ± 0.60
Canes Venatici I	74.3	79.8	218	17.42 ± 0.16
Canes Venatici II	113.6	82.7	160	17.82 ± 0.47
Carina	260.1	-22.2	105	17.83 ± 0.10
Cetus II	156.47	-78.53	30	19.10 ± 0.60
Columba I	231.62	-28.88	182	17.60 ± 0.60
Coma Berenices	241.9	83.6	44	19.00 ± 0.36
Draco	86.4	34.7	76	18.83 ± 0.12
Draco II	98.29	42.88	24	19.30 ± 0.60
Eridanus II	249.78	-51.65	330	17.28 ± 0.34
Eridanus III	274.95	-59.6	95	18.30 ± 0.40
Fornax	237.1	-65.7	147	18.09 ± 0.10
Grus I	338.68	-58.25	120	17.90 ± 0.60
Grus II	351.14	-51.94	53	18.70 ± 0.60
Hercules	28.7	36.9	132	17.37 ± 0.53
Horologium I	271.38	-54.74	87	18.40 ± 0.40
Horologium II	262.48	-54.14	78	18.30 ± 0.60
Hydra II	295.62	30.46	134	17.80 ± 0.60
Indus II	354	-37.4	214	17.40 ± 0.60
Kim 2	347.2	-42.1	69	18.60 ± 0.40
Leo I	226	49.1	254	17.64 ± 0.14
Leo II	220.2	67.2	233	17.76 ± 0.2
Leo IV	265.4	56.5	154	16.40 ± 1.15
Leo V	261.86	58.54	178	17.65 ± 0.97
Pegasus III	69.85	-41.81	205	18.30 ± 0.94
Phoenix II	323.69	-59.74	95	18.30 ± 0.40
Pictor I	257.29	-40.64	126	18.10 ± 0.40
Pisces II	79.21	-47.11	182	17.60 ± 0.40
Reticulum II	266.3	-49.74	32	18.68 ± 0.35
Reticulum III	273.88	-45.65	92	18.20 ± 0.60
Sagittarius II	18.94	-22.9	67	18.40 ± 0.60
Sculptor	287.5	-83.2	86	18.58 ± 0.05
Segue 1	220.5	50.4	23	19.12 ± 0.54
Sextans	243.5	42.3	86	17.73 ± 0.13
Triangulum II	140.9	-23.82	30	19.10 ± 0.60
Tucana II	328.04	-52.35	58	18.80 ± 0.40
Tucana III	315.38	-56.18	25	19.30 ± 0.60
Tucana IV	313.29	-55.29	48	18.70 ± 0.60
Tucana V	316.31	-51.89	55	18.60 ± 0.60
Ursa Major I	159.4	54.4	97	18.26 ± 0.28
Ursa Major II	152.5	37.4	32	19.44 ± 0.40
Ursa Minor	105	44.8	76	18.75 ± 0.12
Willman 1	158.6	56.8	38	18.90 ± 0.60

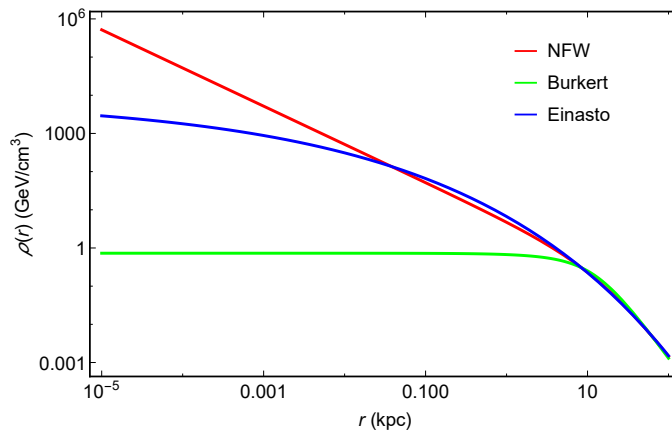


FIG. 1. Galactic dark matter halo density profiles.

IV. EXTRAGALACTIC γ -RAY BACKGROUND AND EXTRAGALACTIC γ -RAYS FROM DARK MATTER ANNIHILATIONS

In this section, we compute the defused extragalactic γ -ray flux from dark matter annihilation and compared with different possible backgrounds. Here we like to mention that, the saying models (Model I and Model II as described earlier) are adopted for particle dark matter candidate and the same set of model parameter values given in Table I and Table III re used for computing the dark matter annihilation cross-section in extragalactic case also. The γ -ray flux from dark matter annihilation could have extragalactic origins too and probing such γ -rays could be effective not only for indirect detection of extragalactic DM but also to understand their origins [7, 11, 27, 44, 45, 48, 56, 58, 59]. But whether such γ -ray signals can be identified by terrestrial telescopes depend on the background γ -rays from different other types of extragalactic sources. Therefore, to study the γ -rays from extragalactic dark matter annihilation, one needs to estimate the flux from other possible sources that can contribute to the backgrounds for such observations.

In order to explore the possibilities that γ -ray signals from the extragalactic dark matter annihilations (indirect DM signals) could be detected with significance, we also compute the γ -ray signals from other possible non-DM origins of extragalactic γ -rays. Such non-DM origins include BL Lac objects, quasars, pulsars, Gamma Ray Bursts (GRB) etc. For many of these sources, the natures of spectra are found to follow roughly a power law. A list of such sources and the corresponding γ -ray flux (power law or other forms) from these sources are furnished later in Table V.

The satellite borne experiment namely *Fermi*-LAT furnished their observed results for extragalactic γ -ray flux. In this section, we compute the sum of the γ -rays from extragalactic DM annihilations (for each of the DM candidate in Model I and Model II) and from other possible non-DM sources. We then compare our results with those observed by *Fermi*-LAT [1, 4].

The rate of photons emitted from volume element dV from the sky depends on several factors mainly the halo mass function dn/dM as a function of mass M and redshift z , the differential photon energy spectrum $\frac{dN_\gamma}{dE}(E, M, z)$, the attenuation factor ($e^{-\tau}$) of the extragalactic γ -rays etc. The rate of photons emitted from volume element dV having energy ranges $E + dE$ and observed by detector having effective area dA (with time interval dt and redshifted energy interval dE such that $dt dE = \left[\frac{dt_0}{1+z}\right] [(1+z)dE_0]$ where t_0 and E_0 are the time and energy respectively at $z = 0$) is given by,

$$dN_\gamma = e^{-\tau} \left[(1+z)^3 \int dM \frac{dn}{dM}(M, z) \times \frac{dN_\gamma}{dE}(E, M, z) \right] \frac{dV dA}{4\pi(R_0 S_k(r))^2} dE_0 dt_0. \quad (6)$$

In the above, the volume element dV is given by

$$dV = \frac{(R_0 S_k(r))^2 R_0}{(1+z)^3} dr d\Omega_{\text{detector}}, \quad (7)$$

where $S_k(r)$ is Universe's spatial curvature appearing in Robertson-Walker metric. The quantity $\frac{dn}{dM}(M, z)$ is the halo mass function where as $\frac{dN_\gamma}{dE}(E, M, z)$ is the photon energy flux. In this case, we consider that the γ -rays are

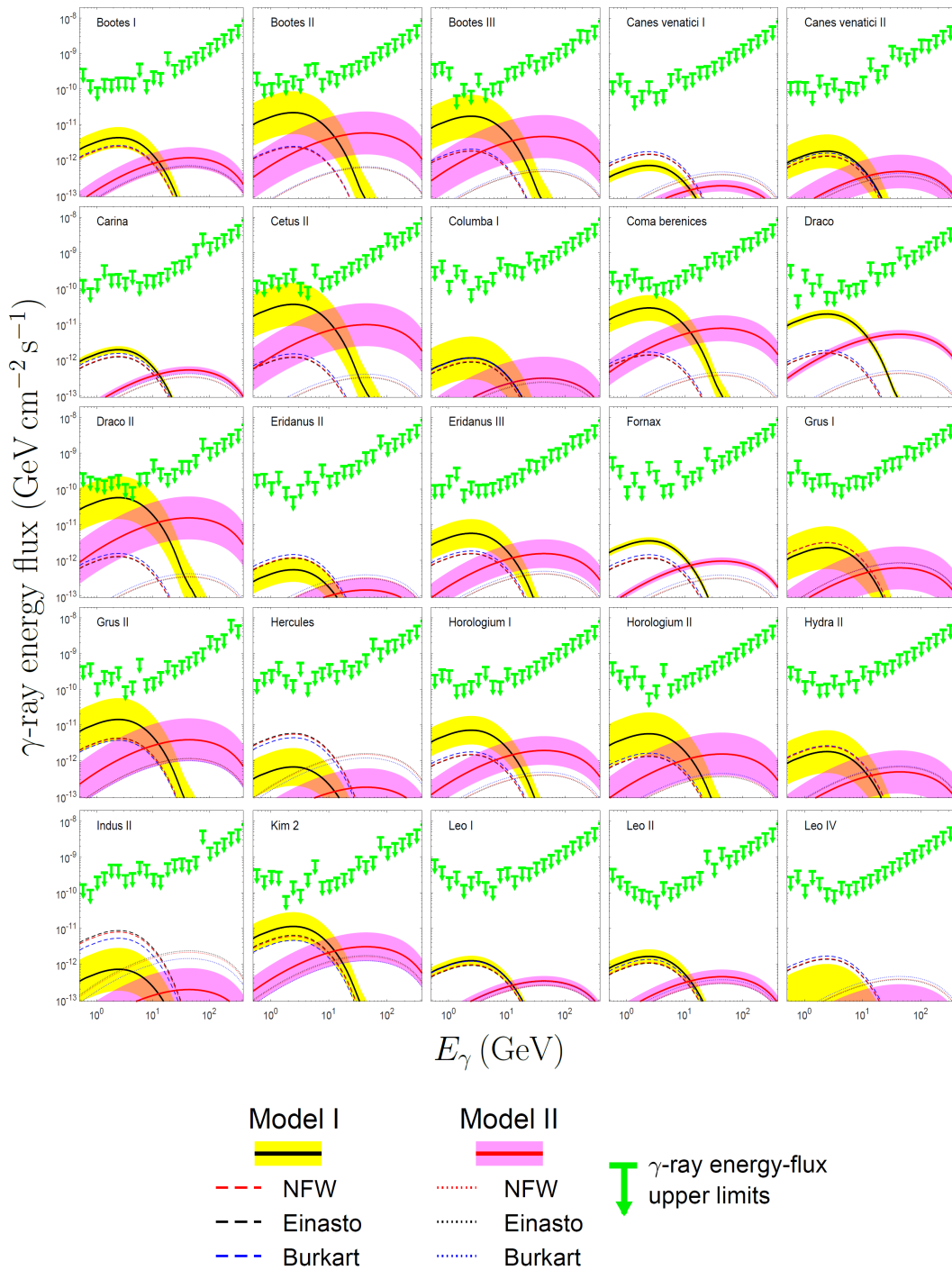


FIG. 2. γ -ray fluxes from dark matter annihilations for each of the dark matter candidates in Model I (50 GeV fermionic WIMP) and Model II (900 GeV Kaluza-Klein dark matter) calculated for each of the 25 dwarf galaxies and their comparisons with experimental upper bounds of γ -ray flux (shown by green coloured downward arrows) for each of the dwarf spheroidals. The flux calculations with the \mathcal{J} factors from Table IV and its uncertainty spreads are shown by black solid line and yellow band respectively when Model I is considered and the same for the DM candidate of Model II are shown by pink solid line and pink band respectively. The \mathcal{J} factors for both Model I and Model II The computed using three dark matter density profiles which are shown with dashed lines and dotted lines of different colours for comparisons. See text for details.

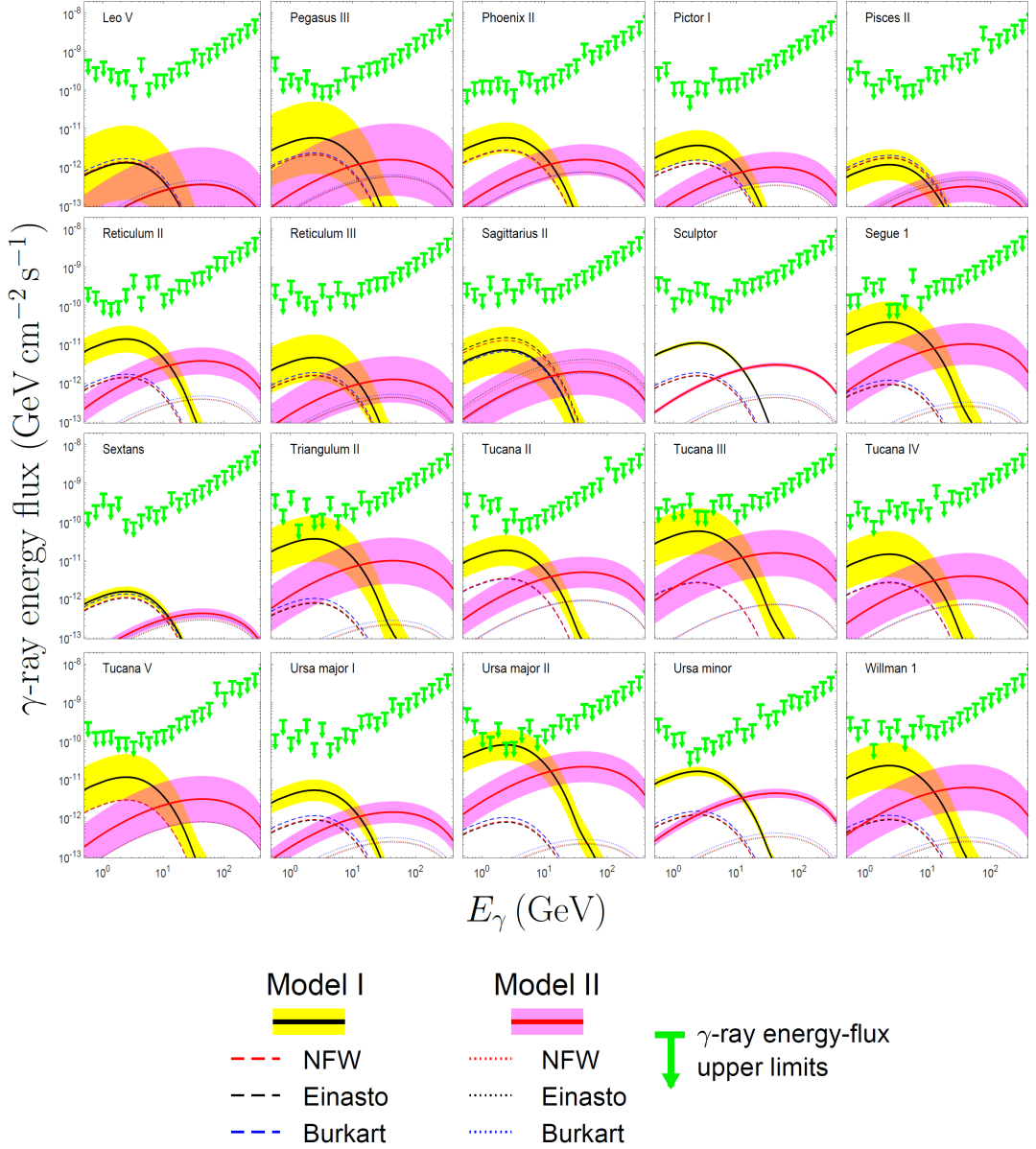


FIG. 3. Same as Fig.2 but for the rest 20 dwarf galaxies. See text for details.

originated as the end product of the dark matter annihilation. Therefore computation of dark matter cross-section is important for the calculation of $\frac{dN_\gamma}{dE}$. The extragalactic γ -rays produced at a redshift z suffers attenuation during its passage through intergalactic medium. This attenuation of extragalactic γ -ray is due to the absorption of high energy γ -rays by extragalactic background light (EBL). Detailed studies for this attenuation are given in Cirelli *et al.* [20] and Fig. 4 is generated following Cirelli *et al.* [20]. This attenuation can be described by an exponential function in terms of the optical depth τ as $e^{-\tau(z, E_0)}$, E_0 being the energy at detection at $z = 0$. The optical depth is related to the pair production of baryonic matter, photon-photon scattering in ambient photon background radiation (PBR) and photon-photon pair production [20]. In Fig. 4 we have shown the dependence of the attenuation factor on redshift (z) and the energy E_0 at detection ($z = 0$).

The PBR depends on the Cosmic Microwave Background (CMB), the intergalactic stellar light and the secondary Infrared (IR) radiation. The Ultraviolet (UV) background can be originated from intergalactic stellar light. These stellar light may come from the massive and hot stars that were ignited at very low redshift. The two models of UV background are generally used for the background estimation. One is the “no UV” case where the contribution of the UV is absent, while the other is “relativistic UV”. The latter has been considered in blazar study and it prescribed a

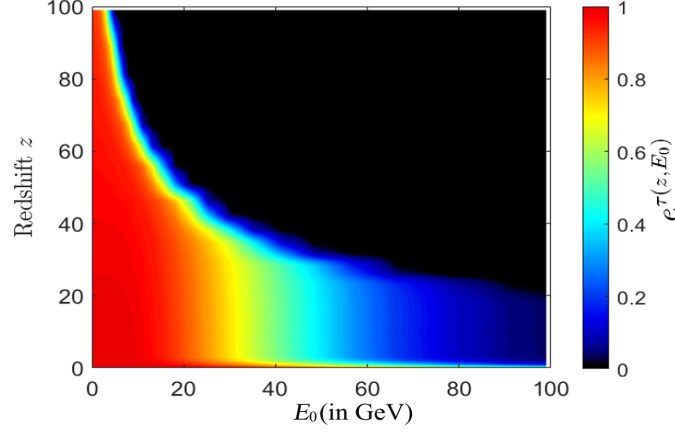


FIG. 4. Variation of optical depth e^τ is described as function of energy E_0 and redshift z . The numerical values of the e^τ is described in the colourbar.

certain value for the UV background proton density. But this value is lower than the values estimated in many of the other earlier analyses [26]. In this work, a significant amount of contribution of the UV background has been taken into account as described in [23, 26]. The diffuse extragalactic γ -ray flux due to DM annihilation is written as,

$$\begin{aligned} \frac{d\phi_\gamma}{dE_0} &= \frac{dN_\gamma}{dAd\Omega dt_0 dE_0} \\ &= \frac{c}{4\pi} \int dz \frac{e^{-\tau(z, E_0)}}{H_0 h(z)} \int dM \frac{dn}{dM}(M, z) \\ &\quad \frac{dN_\gamma}{dE}(E_0(1+z), M, z), \end{aligned} \quad (8)$$

where c is the speed of light in vacuum, H_0 denotes the Hubble constant at the present epoch and M is the dark matter halo mass. For spatially flat Universe ($\Omega_k = 0$), $h(z) = \sqrt{\Omega_m(1+z)^3 + \Omega_\Lambda}$, where Ω_i ($i = m, \Lambda, k$) represents the density parameter for matter (M) or dark energy (Λ) or curvature (k). The halo mass function $\frac{dn}{dM}$ is expressed in terms of the fluctuation, the overdensity in structure formation etc. Denoting $\sigma^2(M)$ to be the variance of the linear density field (rms density = σ) the mass function $f(\sigma)$ extrapolated to redshift z can be written following Press-Schechter model [50] as,

$$f(\sigma) = \sqrt{\frac{2}{\pi}} \frac{\delta_c}{\sigma} \exp\left(\frac{-\delta_c^2}{2\sigma^2}\right). \quad (9)$$

This expression arises out of the following assumption. After smoothening the linear density perturbations over a mass scale M , if in a fraction of space this smooth density field exceeds a threshold δ_c then this fraction of space collapses with mass greater than M . This δ_c is called critical overdensity for collapse¹. In other word, this is the critical value of initial overdensity that is required for collapse at z . This mass function f is also written in terms of a quantity ν where $\nu (= \delta_c/\sigma)$ is the overdensity in units of rms density σ . The ratio ν is related to mean square mass fluctuation $\sigma^2(M)$ that is also caused by the non-linear growth of fluctuation. The distribution $f(\nu)$ is the distribution of mass in isolated halos at a given epoch and is related to number densities of halos². The mass density function $\frac{dn}{dM}(M, z)$ is written as [50],

$$\frac{dn}{dM} = \frac{\rho_{0,m}}{M^2} \nu f(\nu) \frac{d \log \nu}{d \log M}, \quad (10)$$

where $\rho_{0,m}$ is the matter density of the comoving background ($\rho_{0,m} = \rho_c \Omega_m (1+z)^3$, ρ_c is the critical density of the Universe), the ratio $\nu = \delta_c/\sigma(M)$ as discussed, where δ_c ($\simeq 1.686$, [32, 47]) is the critical overdensity for spherical

¹ f is also defined as $f(\sigma, z) = \frac{M}{\rho_0} \frac{dn(M, z)}{d \ln \sigma^{-1}}$ where n signifies the halo abundance with mass $< M$ at redshift z and ρ_0 be the mean density of the Universe at that redshift [32]

² Press and Schechter proposed an ellipsoidal collapse model where the aspects of non spherical collapse are also addressed along with the spherical collapse. In this scenario, the critical overdensity (δ_{sc}) for spherical collapse is replaced by (δ_{ec}) the same for ellipsoidal collapse. These are related as $\delta_{ec}(\sigma, z) = \delta_{sc} \left(z \left(1 + \beta \left(\frac{\sigma^2}{\delta_{sc}^2(z)} \right)^\gamma \right) \right)$ with $\beta = 0.47$ and $\gamma = 0.615$ [54]. For massive objects however $\sigma/\delta_{sc} < 1$ and $\delta_{ec}(\sigma, z) \simeq \delta_{sc}(\sigma, z)$

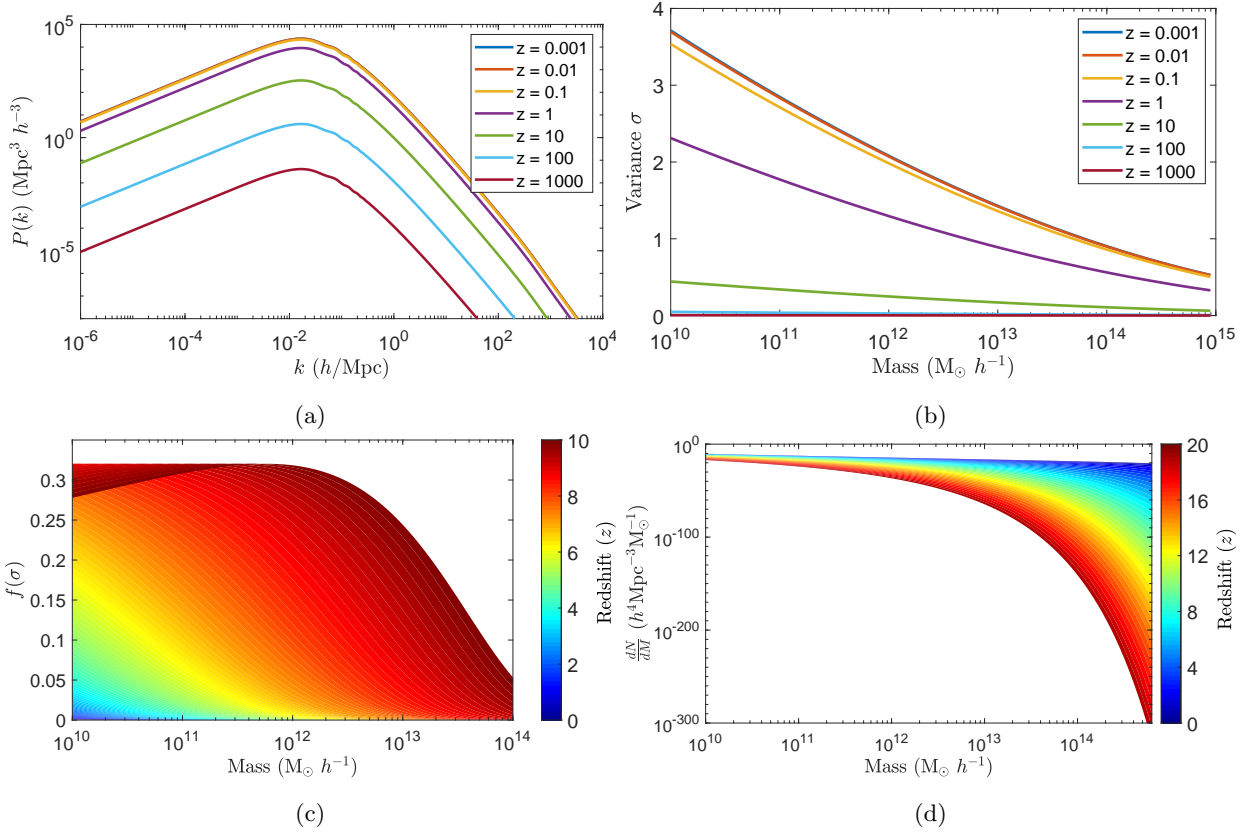


FIG. 5. (a) Fraction of mass collapsed ($f(\sigma)$) for different redshifts z and halo masses M according to the Sheth–Tormen model. (b) Variation of $\frac{dN}{dM}$ with halo mass M for different redshift z . (c) Variance σ of the density perturbations with halo mass for different redshifts (z). (d) Variation of the linear power spectrum $P(k)$ of matter density perturbations with the wave number k for different redshifts (z).

collapse and $\sigma^2(M)$ is the variance of density fluctuations of a sphere containing mass M ($M \simeq (4/3)\pi R^3 \rho_c(z_c)$ for collapse halos, R being the comoving length and z_c is the redshift at which the halo collapses). The term $\sigma^2(M)$ can be represented in terms of the power spectrum $P(k)$ of the initial density perturbation as [55],

$$\sigma^2(M) = \frac{1}{2\pi^2} \int_0^\infty d^3k \tilde{W}^2(kR) P(k). \quad (11)$$

In the above, $\tilde{W}(kR)$ is the Fourier transform of the real space top hat window function of radius R ³. The power spectrum is parameterized as $P(k) \propto k^n T^2(k)$ where n is the spectral index and T is a transfer function related to the DM and baryon density in the Universe. Cosmic microwave background data will be useful for its computation. In Fig. 5a we show the variation of $P(k)$ with wave number k for different z values. We also compute how the variance σ varies with halo mass M . These variations are plotted in Fig. 5b for the same set of z values as in Fig. 5a. The multiplicity function $f(\nu)$ in Eq. 10 is computed using the relation [55],

$$\nu f(\nu) = 2A \left(1 + \frac{1}{\nu'^{2p}}\right) \left(\frac{\nu'^2}{2\pi}\right)^{1/2} \exp\left(-\frac{\nu'^2}{2}\right); \quad (12)$$

where $\nu' = \sqrt{a\nu}$. Fitting the Eq. 10 with N -body simulation of Virgo consortium [31] the numerical values of a ($= 0.707$) and $p = 0.3$ can be obtained. The value of the parameter A in the above equation is adopted as $A = 0.322$ [55]. In terms of σ the mass function $f(\sigma)$ is written as (with $\nu = \delta_c/\sigma(M)$)

$$f(\sigma) = A \sqrt{\frac{2a}{\pi}} \left[1 + \left(\frac{\sigma^2}{a\delta_c^2}\right)^P\right] \frac{\delta_c}{a} \exp\left[-\frac{a\delta_c^2}{2\sigma^2}\right]. \quad (13)$$

³ $\tilde{W}(kR) = 3 \frac{(\frac{\sin kR}{kR} - \cos kR)}{(kR)^2}$

The function $f(\nu)$ as well as the numerical values for ν can be computed by using Eq. 12. The variations of the mass collapse function ($f(\sigma)$) in the ellipsoidal models with the halo mass M for several values of redshift z (0-10) are demonstrated in Fig. 5c. Fig. 5d describes the variations of the considered halo mass function $\frac{dn}{dM}$ of Sheth-Torman model [55] with redshift z and the halo mass M . Note that, Fig. 4 is just a demonstrative plot for the variation of optical depth with energy and redshift. In order to generate this demonstrative plot, all the necessary numerical calculations have been executed by performing HMFcalc [40] code.

According to the Λ CDM cosmological model, the DM halos are formed in the bottom-up sequence. In this approach, initially the small clumps of matter forms in the presence of a tiny density fluctuation zones having a very high gravitational impact. This small scale structures grow into the larger ones, eventually forming the larger scale structures like the DM halos. The DM density profile of a DM halo as per the suggestion of the N-body simulation can be written as $\rho(r) = \rho_s g(r/r_s)$, where r_s and ρ_s indicate the scale radius and the scale density for a particular halo model respectively. For the halo profile we have chosen NFW halo profile [41, 42] depending on which we can explain the nature of the function $g(r/r_s)$ (NFW halo profile has been mentioned in Table II). The mass of any DM halo contained within the radius r_h is given as

$$M_h = 4\pi\rho_s r_h^3 f(r_h/r_s), \quad (14)$$

where $f(x) = x^3[\ln(1+x)^{-1} - (1+x)^{-1}]$. The NFW profile has two parameters namely a characteristic inner radius r_s and a characteristic inner density ρ_s [60]. One of these characteristic parameter can be replaced by virial radius or virial mass where, virial mass M_{vir} is

$$M_h = M_{\text{vir}} = \frac{4\pi}{3} \Delta_{\text{vir}} \bar{\rho}(z) R_{\text{vir}}^3, \quad (15)$$

where $\Delta_{\text{vir}} \bar{\rho}(z)$ is the mean density in the virial radius R_{vir} and Δ_{vir} is the critical over density at virialisation. In the above, $\bar{\rho}(z)$ is the mean Universal density. For the flat Universe ($\Omega_k = 0$), $\Delta_{\text{vir}}(z)$ takes the form [16]

$$\Delta_{\text{vir}} \simeq (18\pi^2 + 82d - 39d^2), \quad (16)$$

with $d \equiv d(z) = \frac{\Omega_m(1+z)^3}{(\Omega_m(1+z)^3 + \Omega_\Lambda)} - 1$ $\left(d(z) \equiv \Omega(z) - 1 = \frac{\Omega_m(1+z)^3}{E(z)^2} - 1, \text{ where } E(z) = \frac{H(z)}{H_0} \right)$.

The γ -ray energy spectrum $\frac{dN}{dE}$ depends on the halo profile which is taken to be NFW profile in the present calculations. The shape of the profile can be alternatively described in terms of a concentration parameter. As the name suggests this parameter is about the concentration of matter in the halo at different positions and hence is an effective alternative for the description of the shape of the halo density profile. In general, the concentration parameter is formally expressed in terms of the virial radius R_{vir} as $c_{\text{vir}} = \frac{R_{\text{vir}}}{r_s^{(-2)}}$ where $r_s^{(-2)}$ is the radius at which the logarithmic slope of the density profile is -2 $\left(\frac{d \log(\rho)}{dr} = -2 \right)$ [33]. Considering the characteristic radius r_s of the halo to be the radius $r_s^{(-2)}$ and defining $x = \frac{r}{r_s^{(-2)}}$, the NFW density profile (Table II) takes the form $\rho(r) = \rho_s g(r/r_s) = \frac{\rho_s}{x(1+x^2)}$. In the present computation, an r -dependent form is adopted as $c_{\text{vir}} r_{-2} = \frac{R_{\text{vir}}}{r}$, where $r_{-2} = \frac{r_s^{(-2)}}{r_s}$. With this the γ -ray energy spectrum $\frac{dN_\gamma}{dE}(E_0(1+z), M, z)$ for the γ -ray (Eq. 8) (induced by the dark matter annihilation with annihilation cross-section $\langle \sigma v \rangle$) emitted from a halo of mass M at redshift z can be written as,

$$\frac{dN_\gamma}{dE}(E, M, z) = \frac{\langle \sigma v \rangle}{2} \frac{dN_\gamma(E)}{dE} \int dc'_{\text{vir}} \mathcal{P}(c'_{\text{vir}}) \left(\frac{\rho'}{M_\chi} \right)^2 \int d^3r g^2(r/a). \quad (17)$$

Here, the differential γ -ray spectrum is $\frac{dN_\gamma(E)}{dE}$ and c_{vir} is known as the concentration parameter whose lognormal distribution around a mean value (within 1σ [55]) for halos with mass M is denoted as $\mathcal{P}(c_{\text{vir}})$. We finally have,

$$\frac{dN_\gamma}{dE}(E, M, z) = \frac{\sigma v}{2} \frac{dN_\gamma(E)}{dE} \frac{M}{M_\chi^2} \frac{\Delta_{\text{vir}} \bar{\rho}(z)}{3} \int dc'_{\text{vir}} \mathcal{P}(c'_{\text{vir}}) \frac{(c'_{\text{vir}} r_{-2})^3}{[I_1(c'_{\text{vir}} r_{-2})]^2} I_2(x_{\text{min}}, c'_{\text{vir}} r_{-2}). \quad (18)$$

The integration $I_n(x_{min}, x_{max})$ is given by $I_n(x_{min}, x_{max}) = \int_{x_{min}}^{x_{max}} dx x^2 g^n(x)$. Finally the extragalactic γ -ray flux from DM annihilation takes the form [59]

$$\frac{d\phi_\gamma}{dE_0} = \frac{\sigma v}{8\pi} \frac{c}{H_0} \frac{\rho_0^2}{M_\chi^2} \int dz (1+z)^3 \frac{\Delta^2(z)}{h(z)} \frac{dN_\gamma(E_0(1+z))}{dE} e^{-\tau(z, E_0)}, \quad (19)$$

with

$$\Delta^2(z) \equiv \int dM \frac{\nu(z, M) f(\nu(z, M))}{\sigma(M)} \left| \frac{d\sigma}{dM} \right| \Delta_M^2(z, M) \quad (20)$$

and $\left(c_{\text{vir}} = \frac{R_{\text{vir}}}{r_s^{(-2\gamma)}} \right)$,

$$\Delta_M^2(z, M) \equiv \frac{\Delta_{\text{vir}}(z)}{3} \int dc'_{\text{vir}} \mathcal{P}(c'_{\text{vir}}) \frac{I_2(x_{min}, c'_{\text{vir}}(z, M) r_{-2})}{[I_1(x_{min}, c'_{\text{vir}}(z, M) r_{-2})]^2} (c'_{\text{vir}}(z, M) r_{-2})^3. \quad (21)$$

Two forms for concentration parameter c_{vir} are adopted for the present computation of extragalactic γ -ray flux. The first form is $c_{\text{vir}}(M, z) = k_{200} (\mathcal{H}(z_f(M))/\mathcal{H}(z))^{2/3}$ from Macciò et al.[36] with $k_{200} \simeq 3.9$, $\mathcal{H}(z) = H(z)/H_0$ and $z_c(M)$ is the effective redshift when a halo with mass M is formed. The second form $c_{\text{vir}}(M, z) = 6.5 \mathcal{H}(z)^{-2/3} (M/M_*)^{-0.1}$, $M_* = 3.37 \times 10^{12} h^{-1} M_\odot$ follows from a power law model ([36, 43]). In what follows we refer this second form for C_{vir} as ‘‘Power law model for C_{vir} ’’ while the former form for C_{vir} as ‘‘Macciò et al. model for C_{vir} ’’. The dark matter substructure within a halo may form bound subhalos. The minimum mass for such subhalos are denoted by M_{min} . This minimum mass M_{min} for such subhalos are determined from the decoupling temperature of dark matter. Two values of minimum subhalo mass namely $M_{\text{min}} = 10^{-6} M_\odot$ and $10^{-9} M_\odot$ [14, 38] are chosen.

We use Eqs. 6-20 to compute the extragalactic γ -ray flux (Eq. 18) induced by annihilation of dark matter. As mentioned, in order to explore the possibilities that the extragalactic γ -rays could be indirect dark matter signal, the calculations are performed for each of the two particle dark matter candidates followed from the two particle dark matter models considered in this work (similar to what has been described in Section III for the case pf dwarf galaxies). We mention here that for the dark matter models, we adopt exactly the same framework and the numerical values of the parameters (such as couplings) as used for the computation related to the γ -ray fluxes of the dwarf galaxies described in Section II. While one is a 50 GeV dark matter – the WIMP component of a two component WIMP-FImP dark matter model (Model I) the other (Model II) is a 900 GeV Kaluza-Klein (KK) dark matter inspired by extra dimensional models (see Section I).

We also estimate the background flux from different possible extragalactic astrophysical sources. The diffuse γ -ray background may include contributions from BL Lacertea objects (BL Lacs), flat spectrum radio quasars (FSRQs), millisecond pulsars (MSPs), star forming galaxy (SFG), Fanarof-Riley (FR) radio galaxies of type I (FRI) and type II (FRII), ultra high energy cosmic rays (UHECRs), γ -ray bursts (GRBs), star burst galaxy (SBG), ultra high energy protons interacting with the inter-cluster material (UHEp ICM) and gravitationally induced shock waves (IGS). These along with the nature of their empirical nature (power spectra [57]) are tabulated in Table V.

The sum total of the calculated γ -ray flux and the background in case of two dark matter models considered are shown in Figs. 6-9. While the computed results with Model I are given in Figs. 6-7, in Figs. 8-9 we plot the results for Model II. In all the figures, however the extragalactic backgrounds from each of the possible non-DM sources (Table V) are shown. The results computed with each of the two chosen values of minimum subhalo mass ($M_{\text{min}} = 10^{-6} M_\odot$ and $M_{\text{min}} = 10^{-9} M_\odot$) are shown in Fig. 6 and Fig. 7 for the case of Model I and in Fig. 8 and Fig.9 when computations are made for the KK dark matter (Model II).

In all the Figs. 6-9, the sum total of the computed extragalactic γ -ray flux (assumed to have originated from dark matter annihilation) and the background contributions (Table V) are plotted for DM Model I and DM Model II as be the case. The observational results of *Fermi*-LAT [1, 4] experiment is also shown for comparison. It is seen from Figs. 6-9 that for both Model I and Model II of dark matter, the sum total of calculated flux (both with $M_{\text{min}} = 10^{-6} M_\odot$ and $M_{\text{min}} = 10^{-9} M_\odot$) and background is always lower than the *Fermi*-LAT results for both the chosen values of M when the ‘‘Macciò et al. model for C_{vir} ’’ is used for the calculation of γ -ray flux from DM annihilation (Fig. 6 and Fig. 8) and hence no γ -ray signal from possible extragalactic DM annihilation can be detected above the background. The fluxes only due to the dark matter annihilation (no background) computed with each of the two chosen values of M_{min} are also shown in Figs. 6-9 by dashed plots. For all the cases considered in Figs. 6-9 for DM candidates in Model I

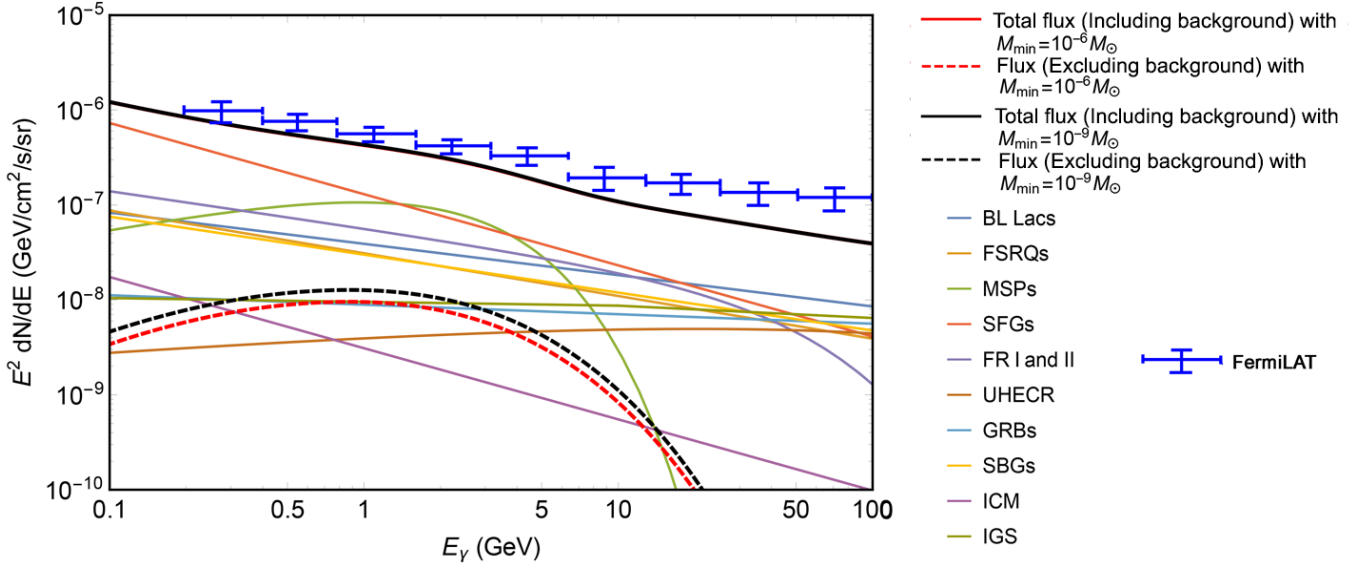


FIG. 6. Observed extragalactic γ -ray fluxes by *Fermi*-LAT compared with the total γ -ray fluxes obtained from the DM annihilation for Model-I DM and other possible non-DM γ -rays extragalactic sources. For the flux calculation, we have taken into account concentration parameter (c_{vir}), which is adopt from Macciò et al. See text for details.

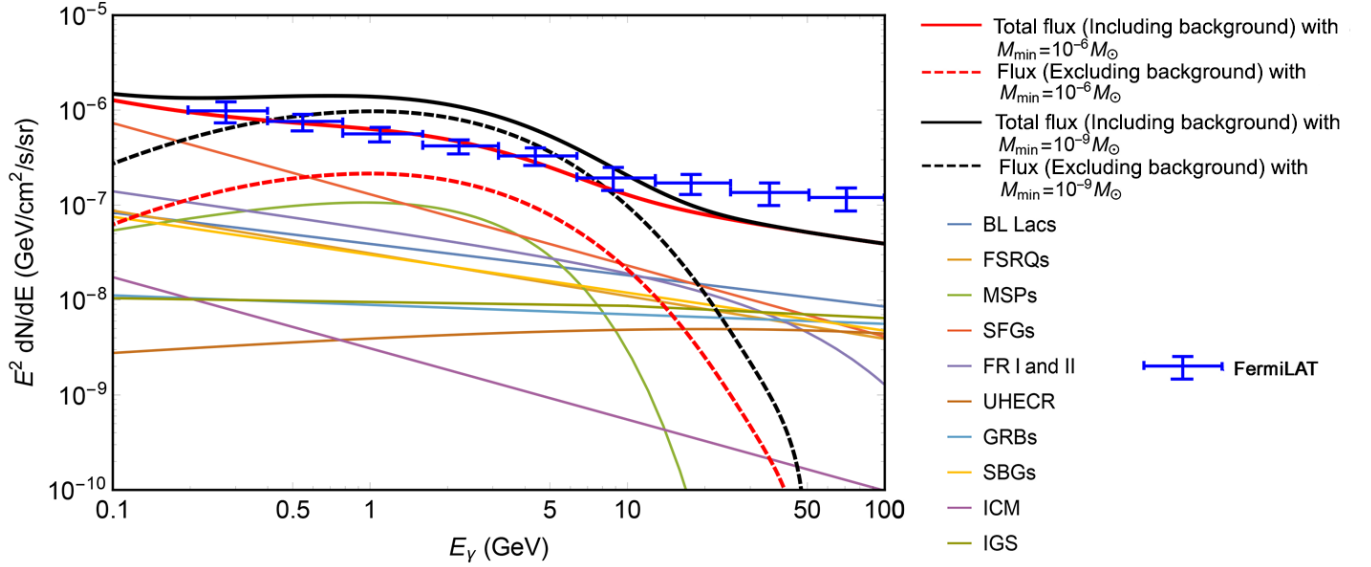


FIG. 7. Observed extragalactic γ -ray fluxes by *Fermi*-LAT compared with the total γ -ray fluxes obtained from the DM annihilation for Model-I DM and other possible non-DM γ -rays extragalactic sources. In this case the power law for c_{vir} is used for the computation of flux. See text for details.

and Model II, it is observed that the calculated flux with $M_{\text{min}} = 10^{-9} M_{\odot}$ always lie above than when computed with $M_{\text{min}} = 10^{-6} M_{\odot}$. From Fig. 7 and Fig. 9, it is seen that the computed γ -ray flux (added with the background from non-DM sources) with “Power law model for C_{vir} ” and $M_{\text{min}} = 10^{-9} M_{\odot}$ (solid black line) goes beyond the *Fermi*-LAT data upto around $E_{\gamma} = 10$ GeV for Model I (Fig. 7). Even only the computed flux (without the background) with $M_{\text{min}} = 10^{-9} M_{\odot}$ goes beyond the *Fermi*-LAT data within certain γ -energy range (Fig. 7).

Similar trends are also seen for the case of KK dark matter also (Fig. 8 and Fig. 9). From Fig. 8, one sees that when “Macciò et al. model for C_{vir} ” is considered the total computed flux (including non-DM background) always lies below the observed flux by *Fermi*-LAT in the considered range for E_{γ} . But here also the flux with $M_{\text{min}} = 10^{-9} M_{\odot}$ are closer to the observed results than when computed with $M_{\text{min}} = 10^{-6} M_{\odot}$. Interesting results are obtained for KK dark matter when “Power law model for C_{vir} ” is used in the calculations (Fig. 9). In Fig. 9 one observes that the

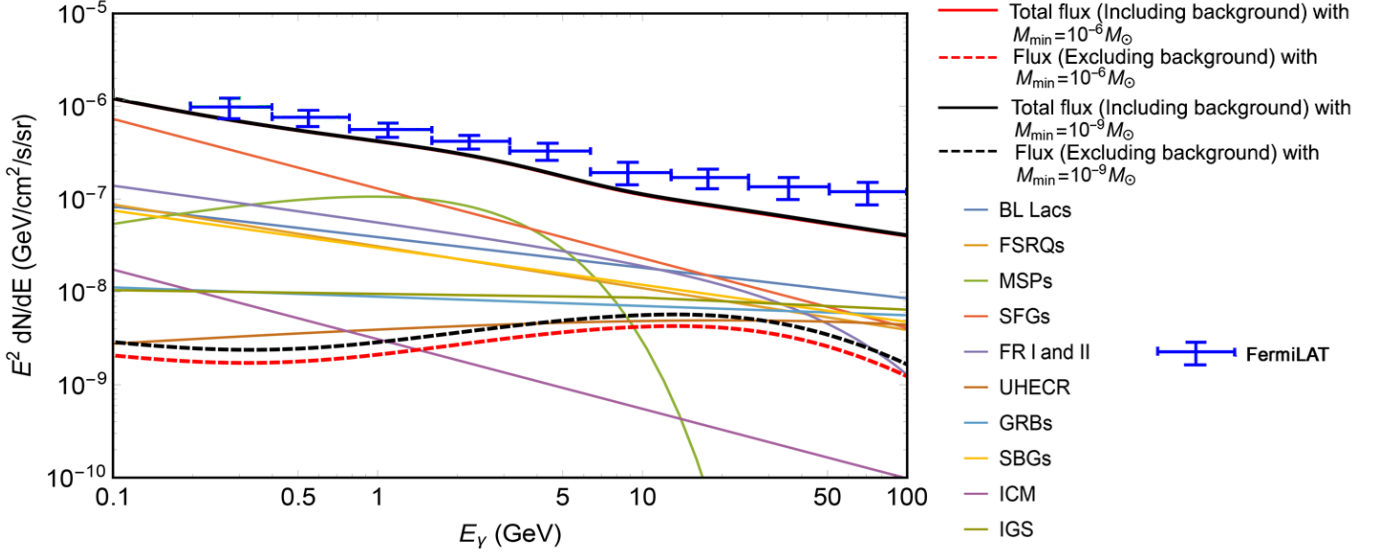


FIG. 8. Same as Fig. 6 but for the DM candidate of Model II. See text for details.

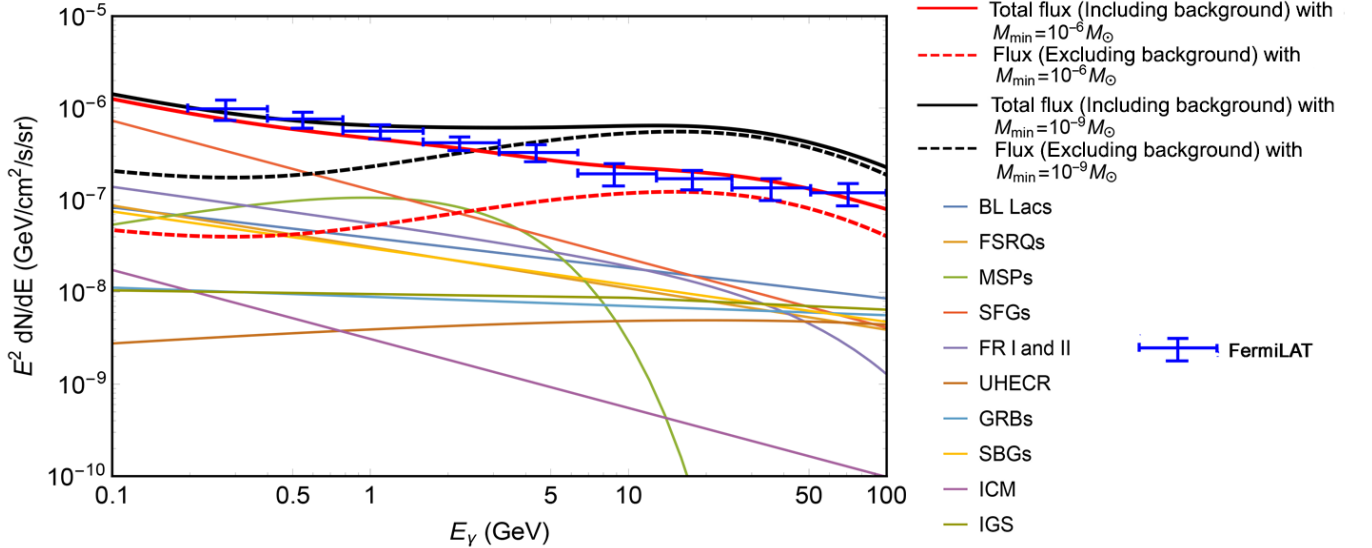


FIG. 9. Same as Fig. 7 but for the DM candidate of Model II. See text for details.

total calculated flux (including the background) with $M_{\min} = 10^{-6}M_{\odot}$ agrees very well with the *Fermi*-LAT results for almost the whole considered range of E_{γ} upto the energy ~ 1 GeV. The total flux, when $M_{\min} = 10^{-9}M_{\odot}$, agrees with *Fermi*-LAT in lower energy region (upto ~ 1 GeV). Comparing with Fig. 7 (similar case for Model I) it appears that the extragalactic γ -rays from the annihilation of KK dark matter in extra dimensional model better agrees with experimental results than the WIMP DM of Model I with dark matter mass of 50 GeV. It can also be observed from Figs. 6-9 that “Power law model for C_{vir} ”, the concentration parameter, is more suited than the “Macciò et al. model for C_{vir} ” in the present calculations.

V. SUMMARY AND DISCUSSIONS

In this work, we explore the observational upper limits of γ -ray flux from 45 dwarf spheroidal galaxies and relate these to the γ -rays that could be produced from annihilation of dark matter in dSphs. From the mass to luminosity ratios, it appears that dSphs could be rich in dark matter and the dark matter can produce γ -rays via the annihilation

TABLE V. The contributions of non-dark matter sources to the extragalactic γ ray background.

Non-DM source	$\frac{dN}{dE}$ in $\text{GeV}^{-1}\text{cm}^{-2}\text{s}^{-1}\text{sr}^{-1}$
BL Lacs	$3.9 \times 10^{-8} E_\gamma^{-2.23}$
FSRQ	$3.1 \times 10^{-8} E_\gamma^{-2.45}$
MSP	$1.8 \times 10^{-7} E_\gamma^{-1.5} \exp\left(-\frac{E_\gamma}{1.9}\right)$
SFG	$1.3 \times 10^{-7} E_\gamma^{-2.75}$
FR I and FR II	$5.7 \times 10^{-8} E_\gamma^{-2.39} \exp\left(-\frac{E_\gamma}{50.0}\right)$
UHECR	$4.8 \times 10^{-9} E_\gamma^{-1.8} \exp\left[-\left(\frac{E_\gamma}{100.0}\right)^{0.35}\right]$
GRB	$8.9 \times 10^{-9} E_\gamma^{-2.1}$
SBG	$0.3 \times 10^{-7} E_\gamma^{-2.4}$
UHEp ICM	$3.1 \times 10^{-9} E_\gamma^{-2.75}$
IGS	$0.87 \times 10^{-10} \times \begin{cases} \left(\frac{E_\gamma}{10.0}\right)^{-2.04} & \text{for } E_\gamma < 10\text{GeV} \\ \left(\frac{E_\gamma}{10.0}\right)^{-2.13} & \text{for } E_\gamma > 10\text{GeV} \end{cases}$

process. For our analysis, we consider two dark matter candidates in two particle dark matter models. One is a two component WIMP-FIMP model of which the WIMP component undergoes annihilation to produce the γ -ray flux. The WIMP component is a Dirac singlet fermion and its additional $U(1)_{\text{DM}}$ charge prevents its interaction with Standard Model (SM) fermions. But the interaction between the WIMP fermion and the SM sector can be occurred via the higgs portal. The benchmark mass for this dark matter is chosen to be 50 GeV for the present analysis. The other particle dark matter chosen for the analysis is Kaluza-Klein (KK) dark matter inspired by models of extra dimensions. In Universal extra dimensional model B^1 , which we have consider as the KK dark matter candidate in this work, is the KK partner of hypercharge gauge boson. This is stable due to the conservation of KK parity $(-1)^{KK}$ where KK is the KK number of the Kaluza-Klein tower related to the extra dimensional momentum. The mass of B^1 that satisfies the dark matter relic density is ~ 900 GeV. In this work, we have taken the mass of B^1 to be 900 GeV which is much higher than the Higgs portal fermionic dark matter in Model I. It appears from the analysis that for both the Higgs portal model and KK model, the dark matter annihilations to γ -rays for 45 dwarf galaxies are well within the observational upper bounds of the γ -ray flux for all the 45 galaxies considered. While the Higgs portal dark matter (Model I) covers a shorter range, the Kaluza-Klein dark matter having higher mass range can probe the γ -ray flux at higher energy range.

We have also extended our analyses for the case of possible extragalactic signature of γ -rays from dark matter annihilations. If detected, such signals could be the indirect extragalactic dark matter signals. For this extragalactic case also, we adopt the same dark matter models and the model parameter values given in Tables I and III and discussed in Sections I and II. But there can be many extragalactic γ -ray sources other than possible dark matter annihilations. These non-DM sources for extragalactic γ -rays originate the background for the γ -rays produced via possible extragalactic dark matter annihilations. We have made an estimation of the flux for such extragalactic sources. The γ -ray flux from dark matter annihilations primarily depends on the annihilation cross-section of the particle dark matter candidate. In addition to this, the parameters which we need to taken into account for the γ -ray flux calculation are the dark matter halo mass function, the density fluctuation in the halo, the linear and non-linear growth of density perturbation and their collapse, the virial radius, the minimum mass M_{min} required for the formation of the subhalo within a DM halo, the γ -ray spectrum ($\frac{dN}{dE}$), the attenuation factor of these γ -rays during it's passage towards a terrestrial detector etc. It is also required to use a feasible model for dark matter halo density profile. In this calculations, NFW density profile has been considered and this NFW density profile is a function of concentration parameter (c_{vir}), which plays a major role to compute the extragalactic γ -ray flux originated from the dark matter annihilation. For the analysis, we adopt two forms for c_{vir} , where one is a power form and the other one is a form given by [36]. We have considered two distinct values foe minimum mass M_{min} , which are $M_{\text{min}} = 10^{-6}M_\odot$ and $M_{\text{min}} = 10^{-9}M_\odot$. The calculations are performed for the case of the fermionic WIMP dark matter in Model I and the Kaluza Klein extra dimensional dark matter candidate in Model II. The computed results are then compared with the observed results for *Fermi*-LAT satellite borne experiments. Our analyses show that the power law choice for c_{vir} yields better results in comparison to the other choice. For the case of power law choice for c_{vir} , the γ -ray flux from the annihilation of fermionic WIMP dark matter of mass 50 GeV in Model I compares well with *Fermi*-LAT data at least upto $E_\gamma \sim 10$ GeV when $M_{\text{min}} = 10^{-6}M_\odot$ and lies above the *Fermi*-LAT (upto $E_\gamma \sim 10$ GeV) when $M_{\text{min}} = 10^{-9}M_\odot$. Better agreements are obtained for the Kaluza Klein dark matter candidate of Universal Extra Dimension model (Model II in this work). The KK dark matter candidate is more massive (~ 900 GeV) than the

WIMP dark matter candidate in Model I (~ 50 GeV). The computed flux for this KK DM candidate (for power law choice of c_{vir}) agrees satisfactorily with the *Fermi*-LAT results for $M_{\text{min}} = 10^{-6} M_{\odot}$ having a wider energy range than in case of the former DM candidate.

The present analyses therefore demonstrate the possibilities of detecting indirect signal of dark matter from extragalactic origins as well as from dwarf spheroidals. The results also indicate that the particle nature of dark matter can be probed from the study of the γ -rays from both dwarf galaxies and extragalactic sources.

ACKNOWLEDGEMENTS

Two of the authors (S.B. and A.H.) wish to acknowledge the support received from St. Xavier's College, Kolkata. One of the authors (A.H.) also acknowledges the University Grant Commission (UGC) of the Government of India, for providing financial support, in the form of UGC-CSIR NET-JRF. One of the authors (MP) thanks the DST-INSPIRE fellowship (DST/INSPIRE/FELLOWSHIP/IF160004) grant by DST, Govt. of India.

DATA AVAILABILITY

The data underlying this article are available in the article.

-
- [1] Abdo, A. A. *et al.*, Phys. Rev. Lett. **104**, 101101 (2010), arXiv:1002.3603 [astro-ph.HE].
- [2] Ackermann, M. *et al.* (Fermi-LAT), JCAP **1509**, 008 (2015), arXiv:1501.05464 [astro-ph.CO].
- [3] Ackermann, M. *et al.*, Physical Review Letters **115**, 231301 (2015), arXiv:1503.02641 [astro-ph.HE].
- [4] Ackermann, M. *et al.* (Fermi-LAT), Astrophys. J. **799**, 86 (2015), arXiv:1410.3696 [astro-ph.HE].
- [5] Ajello, M. *et al.*, The Astrophysical Journal Letters **800**, L27 (2015), arXiv:1501.05301 [astro-ph.HE].
- [6] Albert, A. *et al.* (Fermi-LAT, DES), Astrophys. J. **834**, 110 (2017), arXiv:1611.03184 [astro-ph.HE].
- [7] Ando, S., Phys. Rev. Lett. **94**, 171303 (2005).
- [8] Appelquist, T., Cheng, H.-C., and Dobrescu, B. A., Phys. Rev. **D64**, 035002 (2001), arXiv:hep-ph/0012100 [hep-ph].
- [9] Atwood, W. B. *et al.*, The Astrophysical Journal **697**, 1071 (2009), arXiv:0902.1089 [astro-ph.IM].
- [10] Banik, A. D. and Majumdar, D., Physics Letters B **743**, 420 (2015).
- [11] Bergström, L., Edsjö, J., and Ullio, P., Physical Review Letters **87**, 251301 (2001).
- [12] Biswas, A., Majumdar, D., and Roy, P., JHEP **04**, 065 (2015), arXiv:1501.02666 [hep-ph].
- [13] Boddy, K. K., Kumar, J., Marfatia, D., and Sandick, P., Phys. Rev. D **97**, 095031 (2018).
- [14] Bringmann, T., New Journal of Physics **11**, 105027 (2009).
- [15] Bringmann, T., Calore, F., Di Mauro, M., and Donato, F., Phys. Rev. D **89**, 023012 (2014).
- [16] Bryan, G. L. and Norman, M. L., The Astrophysical Journal **495**, 80 (1998).
- [17] Burkert, A., The Astrophysical Journal **447** (1995), 10.1086/309560.
- [18] Cheng, H.-C., Feng, J. L., and Matchev, K. T., Phys. Rev. Lett. **89**, 211301 (2002), arXiv:hep-ph/0207125 [hep-ph].
- [19] Cholis, I., Hooper, D., and McDermott, S. D., Journal of Cosmology and Astroparticle Physics 10.1088/1475-7516/2014/02/014.
- [20] Cirelli, M. *et al.*, Journal of Cosmology and Astroparticle Physics **2011**, 051 (2011).
- [21] Di Mauro, M., in *5th International Fermi Symposium Nagoya, Japan, October 20-24, 2014* (2015) arXiv:1502.02566 [astro-ph.HE].
- [22] Di Mauro, M. and Donato, F., Phys. Rev. **D91**, 123001 (2015), arXiv:1501.05316 [astro-ph.HE].
- [23] Domínguez, A. *et al.*, Mon. Not. R. Astr. Soc. **410**, 2556 (2011), arXiv:1007.1459.
- [24] Dutta Banik, A., Pandey, M., Majumdar, D., and Biswas, A., The European Physical Journal C **77**, 657 (2017).
- [25] Einasto, J., Astrofiz. Alma-Ata **51** (1965).
- [26] Franceschini, A., Rodighiero, G., and Vaccari, M., Astronomy and Astrophysics **487**, 837 (2008), arXiv:0805.1841.
- [27] Gao, Y.-T., Stecker, F. W., and Cline, D. B., Astronomy and Astrophysics **249**, 1 (1991).
- [28] Hooper, D. and Goodenough, L., Phys. Lett. B **697**, 412 (2011), arXiv:1010.2752 [hep-ph].
- [29] Hooper, D. and Linden, T., Phys. Rev. D **84**, 123005 (2011).
- [30] Hooper, D., Zaharijas, G., Finkbeiner, D. P., and Dobler, G., Phys. Rev. **D77**, 043511 (2008), arXiv:0709.3114 [astro-ph].
- [31] Jenkins, A., Frenk, C. S., Pearce, F. R., Thomas, P. A., Colberg, J. M., White, S. D. M., Couchman, H. M. P., Peacock, J. A., Efstathiou, G., and and, A. H. N., The Astrophysical Journal **499**, 20 (1998).
- [32] Jenkins, A., Frenk, C. S., White, S. D. M., Colberg, J. M., Cole, S., Evrard, A. E., Couchman, H. M. P., and Yoshida, N., Mon. Not. R. Astr. Soc. **321**, 372 (2001), arXiv:astro-ph/0005260 [astro-ph].
- [33] Klypin, A., Yepes, G., Gottlöber, S., Prada, F., and Heß, S., Mon. Not. R. Astr. Soc. **457**, 4340 (2016), <https://academic.oup.com/mnras/article-pdf/457/4/4340/18515365/stw248.pdf>.

- [34] Kong, K. and Matchev, K. T., *Supersymmetry and the unification of fundamental interactions. Proceedings, 14th International Conference, SUSY 2006, Irvine, USA, June 12-17, 2006*, AIP Conf. Proc. **903**, 451 (2007), arXiv:hep-ph/0610057 [hep-ph].
- [35] Lin, H.-N. and Li, X., *Mon. Not. R. Astr. Soc.* **487**, 5679 (2019), <https://academic.oup.com/mnras/article-pdf/487/4/5679/28897927/stz1698.pdf>.
- [36] Macciò, A. V., Dutton, A. A., and van den Bosch, F. C., *Mon. Not. R. Astr. Soc.* **391**, 1940 (2008), arXiv:0805.1926.
- [37] Majumdar, D., *Mod. Phys. Lett.* **A18**, 1705 (2003).
- [38] Martinez, G. D., Bullock, J. S., Kaplinghat, M., Strigari, L. E., and Troppa, R., *JCAP* **0906**, 014 (2009), arXiv:0902.4715 [astro-ph.HE].
- [39] Modak, K. P. and Majumdar, D., *Astrophys. J. Suppl.* **219**, 37 (2015), arXiv:1502.05682 [hep-ph].
- [40] Murray, S., Power, C., and Robotham, A., (2013), arXiv:1306.6721 [astro-ph.CO].
- [41] Navarro, J. F., Frenk, C. S., and White, S. D. M., *Astrophys. J.* **462**, 563 (1996), arXiv:astro-ph/9508025 [astro-ph].
- [42] Navarro, J. F., Frenk, C. S., and White, S. D. M., *The Astrophysical Journal* **490**, 493 (1997), astro-ph/9611107.
- [43] Neto, A. F. *et al.*, *Mon. Not. R. Astr. Soc.* **381**, 1450 (2007).
- [44] Ng, K. C. Y., Laha, R., Campbell, S., Horiuchi, S., Dasgupta, B., Murase, K., and Beacom, J. F., *Phys. Rev. D* **89**, 083001 (2014).
- [45] Oda, T., Totani, T., and Nagashima, M., *The Astrophysical Journal* **633**, L65 (2005).
- [46] Pace, A. B. and Strigari, L. E., *Mon. Not. R. Astr. Soc.* **482**, 3480 (2018).
- [47] Percival, W. J., *Mon. Not. R. Astr. Soc.* **327**, 1313 (2001), arXiv:astro-ph/0107437 [astro-ph].
- [48] Pieri, L., Bertone, G., and Branchini, E., *Mon. Not. R. Astr. Soc.* **384**, 1627 (2008), <https://academic.oup.com/mnras/article-pdf/384/4/1627/2838096/mnras0384-1627.pdf>.
- [49] Planck Collaboration, Aghanim, N., *et al.*, arXiv e-prints, arXiv:1807.06209 (2018), arXiv:1807.06209 [astro-ph.CO].
- [50] Press, W. H. and Schechter, P., *The Astrophysical Journal* **187**, 425 (1974).
- [51] Salucci, P. *et al.*, *Mon. Not. R. Astr. Soc.* **420**, 2034 (2012).
- [52] Sefusatti, E., Zaharijas, G., Serpico, P. D., Theurel, D., and Gustafsson, M., *Mon. Not. R. Astr. Soc.* **441**, 1861 (2014).
- [53] Servant, G. and Tait, T. M. P., *Nucl. Phys.* **B650**, 391 (2003), arXiv:hep-ph/0206071 [hep-ph].
- [54] Sheth, R. K., Mo, H. J., and Tormen, G., *Mon. Not. R. Astr. Soc.* **323**, 1 (2001), arXiv:astro-ph/9907024 [astro-ph].
- [55] Sheth, R. K. and Tormen, G., *Mon. Not. R. Astr. Soc.* **308**, 119 (1999), astro-ph/9901122.
- [56] Stecker, F. W., *The Astrophysical Journal* **223**, 1032 (1978).
- [57] Tavakoli, M., Cholis, I., Evoli, C., and Ullio, P., *JCAP* **1401**, 017 (2014), arXiv:1308.4135 [astro-ph.HE].
- [58] Taylor, J. E. and Silk, J., *Mon. Not. R. Astr. Soc.* **339**, 505 (2003).
- [59] Ullio, P., Bergstrom, L., Edsjo, J., and Lacey, C. G., *Phys. Rev.* **D66**, 123502 (2002), arXiv:astro-ph/0207125 [astro-ph].
- [60] Wechsler, R. H., Bullock, J. S., Primack, J. R., Kravtsov, A. V., and Dekel, A., *The Astrophysical Journal* **568**, 52–70 (2002).